Singular value decomposition based computationally efficient algorithm for rapid dynamic near-infrared diffuse optical tomography

Saurabh Gupta
Department of Instrumentation, Indian Institute of Science, Bangalore 560 012, India

Phaneendra K. Yalavarthy[a)]
Supercomputer Education and Research Centre, Indian Institute of Science, Bangalore 560 012, India

Debasish Roy
Department of Civil Engineering, Indian Institute of Science, Bangalore 560 012, India

Daqing Piao
School of Electrical and Computer Engineering, Oklahoma State University, Stillwater, Oklahoma 74078

Ram M. Vasu
Department of Instrumentation, Indian Institute of Science, Bangalore 560 012, India

(Received 30 June 2009; revised 21 September 2009; accepted for publication 20 October 2009; published 6 November 2009)

Purpose: A computationally efficient algorithm (linear iterative type) based on singular value decomposition (SVD) of the Jacobian has been developed that can be used in rapid dynamic near-infrared (NIR) diffuse optical tomography.
Methods: Numerical and experimental studies have been conducted to prove the computational efficacy of this SVD-based algorithm over conventional optical image reconstruction algorithms.
Results: These studies indicate that the performance of linear iterative algorithms in terms of contrast recovery (quantitation of optical images) is better compared to nonlinear iterative (conventional) algorithms, provided the initial guess is close to the actual solution. The nonlinear algorithms can provide better quality images compared to the linear iterative type algorithms. Moreover, the analytical and numerical equivalence of the SVD-based algorithm to linear iterative algorithms was also established as a part of this work. It is also demonstrated that the SVD-based image reconstruction typically requires $O(NN^2)$ operations per iteration, as contrasted with linear and nonlinear iterative methods that, respectively, require $O(NN^3)$ and $O(NN^6)$ operations, with "NN" being the number of unknown parameters in the optical image reconstruction procedure.
Conclusions: This SVD-based computationally efficient algorithm can make the integration of image reconstruction procedure with the data acquisition feasible, in turn making the rapid dynamic NIR tomography viable in the clinic to continuously monitor hemodynamic changes in the tissue pathophysiology.
[DOI: 10.1118/1.3261029]

Key words: rapid dynamic tomography, near-infrared imaging, singular value decomposition, iterative image reconstruction

I. INTRODUCTION

Near-infrared (NIR) diffuse optical tomography uses a finite set of boundary measurements made on the soft-tissue using light in the spectral range of 600–1000 nm to reconstruct the internal distribution of optical properties.[1] When multiwavelength measurements are available, the optical properties can reveal the spectral, thereby functional, properties of the tissue under investigation. The NIR optical tomography has been most intensively investigated for breast cancer imaging[2–4] and brain function assay.[5–7] Typically, the NIR light is delivered through optical fibers and the transmitted light is also collected through the same or additional fibers that are in contact with the surface of the tissue. Using these measurements, distributions of wavelength dependent absorption and/or scattering coefficients of the tissue are reconstructed using a model-based iterative algorithm.[6] These NIR studies have the advantage of being noninvasive and nonionizing, making it applicable for investigating functional changes in a tissue over a prolonged time.

As the malignant tumor vasculature is known to be different from the benign one, the main aim of the NIR optical tomography has been to noninvasively capture the difference in the vasculature or, more precisely, the dynamics of it as NIR light can penetrate deep tissues. Efforts have been made[8–11] to develop NIR systems capable of acquiring the NIR tomography data at high speed up to the video-rate. These systems use spectrally encoded parallel light delivery to achieve a frame rate of 35 Hz.[9,11] The transmitted light from the boundary of the tissue is acquired through a charge coupled device camera, which is then decoded to recover the data corresponding to specific source-detector locations. As intensity measurements are generally suitable in providing optical absorption coefficient distribution, the scattering co-

efficient is not used as an unknown parameter in rapid dynamic optical tomographic imaging.[9,11,12] Although the data acquisition in these rapid dynamic (video-rate) NIR optical tomography systems has been performed at higher rates (~35 frames/s), the image reconstruction has always been handled off-line due the computational complexity of iterative algorithms.[9,11,12] Typical speed of 10 frames/s to recover the distribution of absorption coefficient is reported in the literature[11] by using a coarse mesh on a Pentium IV 2 GHz CPU. Even though there are methodologies for real-time image reconstructions (integrated with the data acquisition), they often require high-end workstations that have the capability of parallel processing of these algorithms.[13,14] Although attempts have been made to use single-step image reconstruction algorithms,[14,15] they are generally incapable of the much needed optical contrast recovery in dynamic applications.

This work mainly aims at presenting a singular value decomposition (SVD)-based computationally efficient iterative algorithm that can, in principle, obtain the video-rate optical tomographic image reconstruction in-line with the data acquisition. Also, an efficient way of reducing the size of Jacobian, introduced by Eames *et al.*,[16] is combined with the SVD-based algorithm. A systematic comparison of the present reconstruction method with the more traditional ones is provided in order to bring forth the computational efficiency of the former. The SVD-based algorithm is also employed in a reconstruction based on dynamical data (involving increasing absorption over time) acquired from a tissue-mimicking phantom to assess the suitability of the method for being used in-line with the video-rate data. The numerical and experimental studies taken up in this work are restricted to only two-dimensional (2D) domains, which suffice to demonstrate the feasibility of the algorithm in reconstructing rapid dynamic optical images.

II. MATERIALS AND METHODS

II.A. Rapid dynamic NIR diffuse optical tomography: Forward problem

Continuous wave NIR light propagation in thick biological tissues can be modeled using the steady-state diffusion equation,[1] which is an approximation to the radiative transfer equation and is given by

$$-\nabla \cdot D(\vec{r})\,\nabla\Phi(\vec{r}) + \mu_a(\vec{r})\Phi(\vec{r}) = Q_o(\vec{r}), \tag{1}$$

where the optical diffusion and absorption coefficients are denoted by $D(\vec{r})$ and $\mu_a(\vec{r})$, respectively, and $\vec{r}$ denotes the spatial location vector. The light source, represented by $Q_o(\vec{r})$, is modeled as isotropic. $\Phi(\vec{r})$ is the photon fluence rate at a given position $\vec{r}$. We have

$$D(\vec{r}) = (3(\mu_a(\vec{r}) + \mu_s'(\vec{r})))^{-1}, \tag{2}$$

where μ_s' represents the reduced scattering coefficient and is presently considered to be a known parameter (invariable over the domain) in rapid dynamic NIR optical tomography. The finite element method (FEM) is used to solve Eq. (1) and thus generate the modeled data, which is the logarithm of the intensity ($\ln A$) for a given distribution of the absorption coefficient $\mu_a(\vec{r})$.[17–19] Type III boundary condition, which also accounts for the refractive-index mismatch at the boundary,[20] is employed.

II.B. Rapid dynamic NIR diffuse optical tomography: Inverse problem

II.B.1. Levenberg–marquardt (LM) minimization: Nonlinear iterative method

A detailed discussion of the LM method is available in Ref. 21 and it is only briefly reviewed here. The aim of this approach is to minimize the objective functional (Ω), given below, with respect to the absorption coefficient (μ_a)

$$\Omega = \|\ln A^{\text{measured}} - \ln A^{\text{modeled}}\|^2, \tag{3}$$

where $\ln A^{\text{measured}}$ is the measured experimental data and $\ln A^{\text{modeled}}$ is the modeled data (dimension: $NM \times 1$; NM is the number of measurements). Minimization of this objective functional with respect to μ_a is achieved by setting the first-order derivative equal to zero

$$\frac{\partial\Omega}{\partial\mu_a} = \mathbf{J}^T\delta = 0, \tag{4}$$

where $\delta = (\ln A^{\text{measured}} - \ln A^{\text{modeled}})$ is the data-model misfit and $\mathbf{J} = [\partial \ln A^{\text{modeled}}/\partial\mu_a]$ the Jacobian (of dimension $NM \times NN$; NN represents the number of unknowns or, equivalently, the number of FEM nodes). To circumvent the ill-conditioned nature of the problem, the update equation for the optical properties at iteration "i" is regularized leading to

$$\Delta\mu^i = [(\mathbf{J}^{i-1})^T\mathbf{J}^{i-1} + \alpha^i\mathbf{I}]^{-1}(\mathbf{J}^{i-1})^T\delta^{i-1}, \tag{5}$$

where $\Delta\mu^i$ represents the update of the optical absorption coefficient (μ_a) at the ith step, $\mathbf{J}^{i-1}$ represents the Jacobian calculated using optical properties (μ_a) of the previous iteration ($i-1$), and α^i is the (strictly positive) regularization parameter corresponding to the ith iteration, monotonically decreasing with increasing iteration. It typically starts at 1000 and is reduced by a factor of $10^{0.25}$ at each iteration. The stopping criterion for all iterative procedures discussed in this work is chosen so as to ensure that the decrease in the L^2 norm of data-model misfit between successive iterations is less than or equal to 1%. In case of the nonlinear iterative procedure [Eq. (5)], it is known that the error between the expected and reconstructed optical images might increase after a few iterations.[15,22,23] In the case discussed here, such divergence typically occurred after the eighth iteration. Thus for purposes of comparison of the procedures, the reconstructed image at the eighth iteration has been employed.

II.B.2. LM minimization: Linear iterative method

For a set of experimental measurements made in diffuse optical tomography either using a tissue-mimicking phantom or a biological tissue, the data is initially calibrated to remove the detector channel variations and also to provide an initial guess for the iterative procedure.[24,25] Since the initial

TABLE I. Summary of methods discussed in this work along with the corresponding sections and equation numbers.

Method	Section number	Equation number	Jacobian recalculated	Jacobian reduced
Nonlinear	II.B.1	5	Yes	No
Linear iterative	II.B.2	6	No	No
SVD	II.B.3	8	No	No
Linear efficient	II.B.2 and II.B.4	10	No	Yes
SVD efficient	II.B.3 and II.B.4	11	No	Yes

guess is obtained from the average of the measurements made, it is typically close to the background optical properties of the tissue.[24,25] Due to this, we adopt a variation in nonlinear procedure, wherein the Jacobian ($\mathbf{J}$) is only computed once at the initial guess of optical properties (μ_a) and used repeatedly to make the iterative reconstruction procedure computationally efficient. Note that the Jacobian computation is one of the computationally expensive steps [typical order of $O(NN^3)$ flops] in the iterative image reconstruction procedure. This technique is referred to as the "linear iterative method," reflecting the fact that $\mathbf{J}$ is computed only once. The regularized update equation for the optical properties at iteration i for this method is given by

$$\Delta\mu^i = [(\mathbf{J}^0)^T\mathbf{J}^0 + \alpha^i\mathbf{I}]^{-1}(\mathbf{J}^0)^T\delta^{i-1}. \quad (6)$$

Here $\mathbf{J}^0$ represents the Jacobian computed using the initial guess (obtained from the data calibration procedure).

With the LM minimization requiring the regularization parameter (α) to be reduced over every iteration (so it tends to zero asymptotically), each linear iterative step requires αI (appropriately updated) to be added to $\mathbf{J}^T\mathbf{J}$. As the matrix inversion requires $O(NN^3)$ operations,[26] a singular value decomposition of the Jacobian makes the inversion [Eq. (6)] computationally efficient.

II.B.3. SVD: Linear iterative method

Using singular value analysis, the Jacobian can be decomposed as

$$\mathbf{J} = \mathbf{U}\mathbf{S}\mathbf{V}^T, \quad (7)$$

where $\mathbf{U}$ (dimension $NM \times NM$) and $\mathbf{V}$ (dimension $NN \times NN$) are orthonormal matrices containing the singular vectors of $\mathbf{J}$ and the diagonal matrix $\mathbf{S}$ (dimension $NM \times NN$) contains the singular values of $\mathbf{J}$. Combining Eqs. (6) and (7), we can obtain the update $\Delta\mu^i$ for the ith iteration through the equation

$$\Delta\mu^i = V * \sum * U^T * \delta^{i-1}, \quad (8)$$

where Σ is diagonal matrix with the diagonal entries as $S/(S^2+\alpha)$ (Appendix A).

Thus matrix inversion [required on the RHS of Eq. (6)] can be replaced by matrix multiplication. Regularization of $\mathbf{J}^T\mathbf{J}$ [as in Eqs. (5) and (6)] is realized through an addition of α to the denominators of the elements of Σ. This procedure renders the computation of $\Delta\mu$ an $O(NN^2)$ process rather than $O(NN^3)$; further details on number of operations is given in Appendix B.

II.B.4. Jacobian reduction

Recently, Eames *et al.*[16] have developed an efficient Jacobian reduction method to improve the computational efficacy of 3D image reconstruction algorithms. We use the same procedure, wherein the size of the Jacobian is reduced by removing contributions of nodes that are below the total sensitivity threshold. That is, nodal variables that are almost noncontributing (with the nodal position being typically far away from the source and/or the detector) to the total sensitivity are not included as unknowns in the image reconstruction. Accordingly the total sensitivity throughout the imaging domain is computed and a new Jacobian $\tilde{J}_{ij}$ is formed as follows:

$$\tilde{J}_{ij} = \begin{cases} J_{ij} & \text{if } \sum_{i=1}^{NM} J_{ij} >= 5\% \text{ of } M \\ 0 & \text{if } \sum_{i=1}^{NM} J_{ij} < 5\% \text{ of } M \end{cases}, \quad (9)$$

where j corresponds to the node number within the domain and $M = \max(\Sigma_{i=1}^{NM} J_{ij})$. Given a new Jacobian element $\tilde{J}_{ij}$ that corresponds to the total sensitivity for a specific node being zero, the entire column corresponding to that node is removed to produce a much smaller Jacobian matrix. This drastically reduces the number of operations and memory required for computing the update of the optical properties.[16]

The reconstruction scheme involving a reduced Jacobian, as above, is presently referred to as the "efficient method," which is implemented using both linear iterative and SVD-based techniques described earlier. The corresponding "efficient equations" for the linear iterative and SVD methods are given below

$$\text{Linear efficient: } \Delta\mu^i = [(\tilde{\mathbf{J}}^0)^T\tilde{\mathbf{J}}^0 + \alpha^i\mathbf{I}]^{-1}(\tilde{\mathbf{J}}^0)^T\delta^{i-1}, \quad (10)$$

$$\text{SVD efficient: } \tilde{\mathbf{J}} = \tilde{U}S\tilde{V}^T, \quad \Delta\mu^i = \tilde{V} * \sum * \tilde{U}^T * \delta^{i-1}. \quad (11)$$

For a ready reference, the methods used in this work along with its salient features are summarized in Table I. Note that

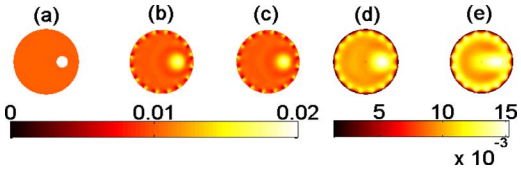

FIG. 1. Reconstruction results using noiseless data. (a) Actual μ_a image. Reconstructed μ_a distribution using (b) nonlinear method and (c) linear iterative method. Reconstructed μ_a image with initial guess (=0.002 mm^{-1}) using (d) nonlinear and (e) linear iterative methods.

computations performed in this work have been carried out on a dual core workstation with 2.66 GHz processor speed and 4 GB memory.

II.C. Simulation and experimental evaluation

For all numerical experiments discussed here, the imaging domain is chosen to be a circle of 86 mm diameter, a dimension representative of a breast imaging system using a ring applicator. The background optical properties are $\mu_a = 0.01\ mm^{-1}$ and $\mu_s' = 1.0\ mm^{-1}$. For the finite element discretizations, one for generating measurements and the other for use in the inversion, we use three-noded triangular elements with the following two mesh densities: (1) 10249 nodes (corresponding to 20160 triangular elements) for the generation of "experimental" data ($\ln A^{\text{measured}}$) and (2) 2773 nodes (corresponding to 5376 elements) for the reconstruction procedure (e.g., in the generation of $\ln A^{\text{modeled}}$). The data collection setup has 16 fibers that are arranged in a circular, equispaced fashion.[27] One fiber is used at a time as the source while the other fibers serve as detectors to generate 240 (15×16) measurement locations or a total of 240 data points for $\ln A$. The sources are modeled as Gaussian with a full width at half maximum of 3 mm to represent the distribution used in a typical experimental setup.[27] The source is also assumed to be located one mean transport length inside the boundary.

Initially, a circular target of radius 7.5 mm with a contrast of 2:1 compared to the background in μ_a placed at location (21, 0) is used to generate the $\ln A^{\text{measured}}$ data using the 10249-node mesh [Fig. 1(a)]. These noise-free numerical measurements are calibrated on the 2773-node mesh and the initial guess for the iterative procedure is obtained from the calibration procedure. Note that the linear iterative procedure [Eq. (6)] is essential for better recovery of optical contrast when compared to a single-step procedure [Eq. (6) for $i=1$].[14,15,28] However, when the initial guess is far away from the actual solution, a comparison of the performance of the nonlinear and linear iterative procedures clearly brings forth the superiority of the nonlinear procedure [Eq. (5)] and hence the need for recomputing the Jacobian in this case. For the same case, a comparative noise tolerance study has also been taken up, wherein the simulated data with added noises of 1%–4% are considered as the $\ln A^{\text{measured}}$.

Next, a comparison of contrast recovery capabilities (corresponding to change in target contrast from 1.5 to 5) of the linear and nonlinear iterative algorithms has been considered. The noise in the data is kept at 1% corresponding to typical data noise level in the experiments. An object with two targets, one near the boundary [location (21,0)] and another in the center [at (0,0)] of the domain, are considered for this purpose. The initial guesses for these iterative schemes are obtained using the calibration procedure referred to earlier.[24,25]

Next a comparison of linear iterative methods (linear iterative, SVD, linear efficient, and SVD efficient; see also Table I) is taken up with data noise level of 1%. For completeness, a comparison of these linear iterative methods with the corresponding nonlinear methods was also performed. We use the L^2 norm of the data-model misfit and root mean square (rms) error between actual and reconstructed absorption coefficient distributions for this comparison. Such a numerical comparison is deemed necessary to show performance equivalence of these linear iterative methods.

As this work pertains to developing a computationally efficient algorithm for rapid dynamic optical tomography, a comparison of computation times per frame for the iterative reconstruction methods, namely, nonlinear, linear efficient, and SVD efficient (Table I), with increasing number of parameters (equivalently, node numbers in the FEM mesh) has also been performed.

Finally, the efficacy of the SVD-based algorithm is assessed in the reconstruction of dynamical changes in absorption in the phantom that were acquired by the video-rate NIR tomography system.[11] This video-rate system has an imaging array of 27 mm in diameter designed to fit a rat's cranium for small animal imaging and 16 equispaced channels for interspersed NIR light delivery and collection. A solid tissue phantom of 27 mm in diameter is placed in the array, ensuring tight coupling of the fibers to the phantom. The solid phantom has a hole of 6.35 mm in diameter for placing bulk intralipid solution wherein the diluted ink is injected steadily. Ink injection starts at shortly after the data acquisition which was at a rate of 35 frames/s.

III. RESULTS

Figure 1 highlights the importance of initial guess being close to the actual solution for the linear iterative method to provide better qualitative and quantitative reconstructed image. Figure 1(a) shows the reference (actual) distribution of μ_a, used to generate the data. Figures 1(b) and 1(c) give the reconstructed images (involving a 2773-node mesh) by using nonlinear and linear iterative methods (Table I), respectively, where the initial guess is obtained from the calibration of the data generated on a 10249-node mesh. Figures 1(d) and 1(e) give the results obtained through nonlinear and linear iterative methods, respectively, for an initial guess of 0.002 mm^{-1} (which is far way from the actual value). It is evident from these results that when initial guess is far away from the true solution, the nonlinear method results in a better recovery of target shape and position than linear iterative methods, as the Jacobian is recomputed at every iteration.

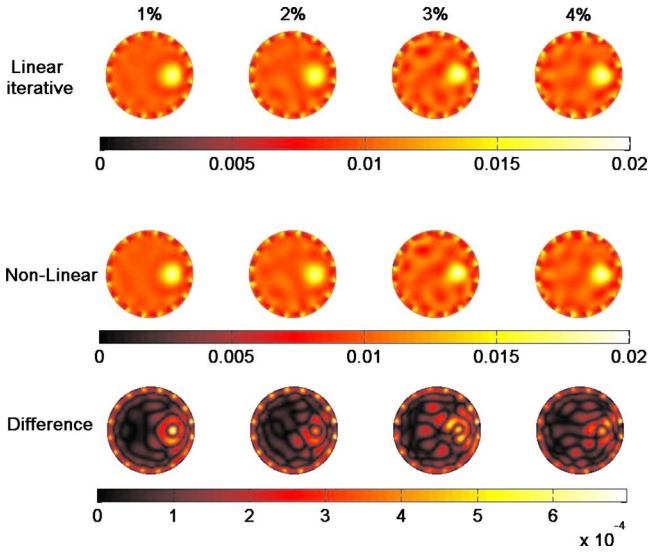

FIG. 2. Comparison of performance of linear iterative and nonlinear methods with increasing noise level (1%–4%, given on top of each column). Top row corresponds to reconstructed image obtained with linear iterative method, middle row corresponds to nonlinear method. Last row gives the difference images between linear iterative and nonlinear methods (top row-middle row).

Next, results pertaining to noise tolerance of linear iterative and nonlinear methods are shown in Fig. 2. The reference μ_a distribution corresponding to Fig. 2 is given in Fig. 1(a). The top row gives the results obtained from the linear iterative method with corresponding data noise level (varying from 1% to 4%) given on top of each image. The middle row of Fig. 2 gives the results obtained from the nonlinear method, corresponding to the distributions shown in the top row. Corresponding difference images (linear iterative-nonlinear) are given in the bottom row of Fig. 2. Note that the initial guess for all the cases in Fig. 2 is obtained from calibration of the noisy data generated using a 10249-node mesh and the reconstructions (along with forward calculations) have been performed using a 2773-node mesh. It is evident from Fig. 2 (last row images) that the difference in

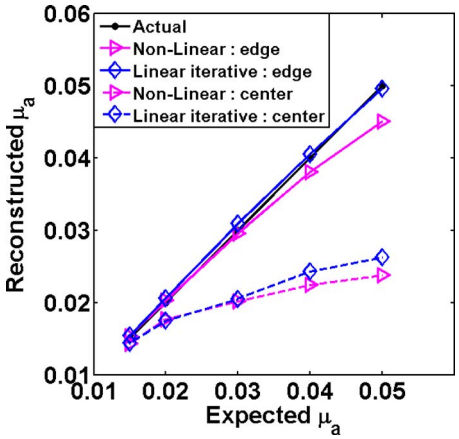

FIG. 3. Plot of expected versus reconstructed μ_a (maximum value in the region) for the target positions (given in the legend of the figure) using both nonlinear and linear iterative methods.

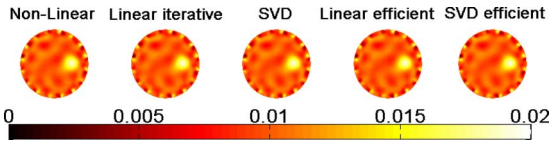

FIG. 4. Reconstructed μ_a distributions using (a) nonlinear, (b) linear iterative, (c) SVD, (d) linear efficient, and (e) SVD efficient methods with 1% noise in the data (salient features of the reconstruction methods are given in Table I). The expected μ_a distribution is given Fig. 1(a).

the reconstructed images using nonlinear and linear iterative method is less than 4% of the reconstructed values.

Results on the contrast recovery via linear iterative and nonlinear methods showing target position dependence are shown in Fig. 3. Initial guess obtained from the calibration of 1% noisy data is used in results presented here. As the sensitivity of measurements (with respect to the parameters to be reconstructed) varies with the distance from the boundary,[29] two target positions (one near the boundary of the domain (21, 0) and another at the origin) are considered in this study. The contrast is varied from 1.5 to 5 times with respect to the background, and the maximum value of recovered μ_a is used to generate these plots. For the same initial guess, the linear iterative method recovers the contrast better. Reconstruction results obtained using the SVD-based linear iterative algorithm and/or with the Jacobian reduction method are given in Fig. 4 [expected μ_a distribution is given in Fig. 1(a)] for data noise level of 1% along with the reconstructed result using nonlinear method. The obtained reconstructed distributions are almost identical in appearance in all five cases, namely, nonlinear, linear iterative, SVD, linear efficient, and SVD efficient (Table I). More closely, Figs. 5(a) and 5(b) give the plots of data-model misfit and rms error in μ_a with respect to the iteration number. Differences in these plots for the linear iterative methods are within the numerical precision of the machine, lending credence to the supposition that linear iterative methods (linear iterative, SVD, linear efficient, and SVD efficient) are not only equivalent analytically, but also identical numerically.

An important result as part of this study is provided in Fig. 6, where the computation time per frame versus the number of unknowns (or FEM nodes) is plotted (semi-log plot) for the nonlinear, linear efficient, and SVD efficient methods discussed herein (Table I). Note that the polynomial

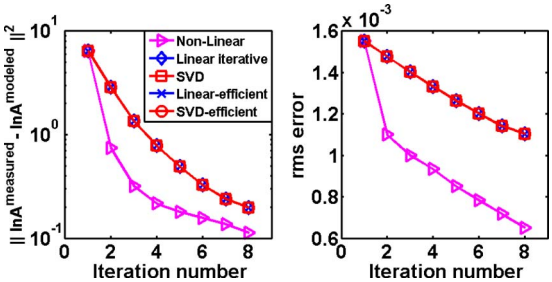

FIG. 5. (a) Plot of iteration number versus L^2 norm of data-model misfit. (b) Plot of iteration number versus rms error between expected and reconstructed μ_a distribution. The corresponding final images are given in Fig. 4.

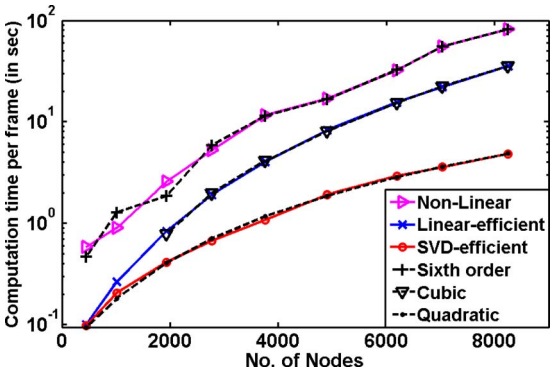

FIG. 6. A semi-log plot of number of nodes (unknown parameters) versus reconstruction time per frame for nonlinear, linear efficient, and SVD efficient methods (given in the legend) described in this work (Table I). Polynomial fits corresponding to each method (Appendix B) are also plotted (dotted lines) in this figure, represented by the legend.

fits corresponding to each method (Appendix B) are also plotted in Fig. 6. In the approaches considered here, the performance of the linear iterative and SVD methods, in their conventional efficient forms, was similar in terms of the computational efficacy; however the details of the comparison are not shown here. The nodal density in the FEM discretization determines, among others, the numerical accuracy of the forward model, consistent with the anticipation that finer FEM mesh (more nodes) typically leads to better reconstruction results.[29] Figure 6 clearly shows that the SVD-based method is computationally more efficient *vis-à-vis* the others for the same number of FEM nodes.

Figure 7 shows an example reconstruction of dynamical data collected on a tissue-mimicking phantom using the SVD-based algorithm. The data are used for reconstructions at ~10 frames/s using the SVD efficient algorithm leading to a 100-fold improvement in reconstruction time compared with the conventional nonlinear reconstruction.[10] Reconstructions using the SVD efficient algorithm at the time-frames of 0–0.85 s (in ~0.1 s time intervals) are shown in Fig. 7(a). The continuous change in the maximum absorption coefficient in the ink-hole region and plateau after 0.7 s is given in Fig. 7(b).

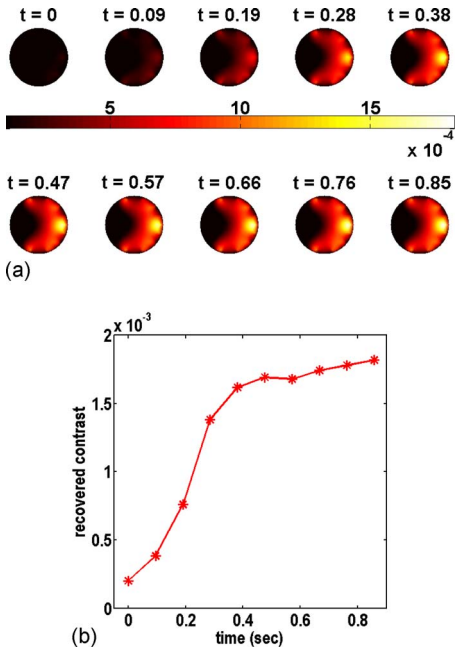

FIG. 7. (a) An example of reconstructed dynamic data set using the SVD method. The corresponding time points are shown at the top of each figure. (b) Recovered μ_a contrast (maximum value in the target region) versus time.

IV. DISCUSSION

Image reconstruction in rapid dynamic NIR tomography is typically performed off-line due to the computational complexity, even though the data can be acquired at speeds up to the video-rate.[8–11] The aim of this work is to demonstrate that an exploitation of the SVD of the Jacobian can make the image reconstruction procedure in sync with the data acquisition, making rapid NIR tomography viable in the clinical setting to either continuously monitor the hemodynamic or dynamical changes in the tissue pathophysiology.

In this work, we have also demonstrated, using experimental data and initial guess obtained therewith, that linear iterative methods can indeed yield reconstructed images of about the same quality and quantification as nonlinear iterative methods, albeit with lesser computational overhead [Figs. 1(b), 1(c), 2, 3, and 6]. However, for initial guesses far away from the actual solution, the nonlinear method will always lead to more accurate reconstruction due to the recomputation of the Jacobian. This is clearly borne out in Figs. 1(d) and 1(e). More specifically, linear and nonlinear iterative methods with the initial guess obtained through the calibration procedure have produced results that are similar (within ~4%), even when the data noise level is increased from 1% to 4% (Fig. 2). This reveals that the recomputation of the Jacobian may not be necessary provided the data calibration enables estimating the initial guess not too far from the actual solution. It should be noted that, for the dynamic reconstruction considered here, after the initial calibration, reconstruction at the *i*th time step can serve as the background distribution for the following time step. Moreover, owing to the time interval between successive frames being too small to result in appreciable variation in contrast, anticipated updates are also likely to be small. Therefore in this case accurate reconstructions using the linear methods should be possible.

In the present context, it is insightful to bring out the difference between linear (single-step) and linear iterative methods reconstructing the contrast changes. There were earlier attempts to use linear methods to recover the optical property distributions.[14,15,28] It is proven that even though single-step methods are capable of detecting the targets (qualitatively) given the background optical property distributions, they are limited in their ability for quantitative recovery.[15,28] Accordingly, in this work, comparisons are limited to linear iterative methods.

Comparison of the contrast recovery between linear and nonlinear iterative methods for data noise level of 1% yields

similar trends (Fig. 3). Note that an experimental setup, with a ringlike source/detector geometry and limited number of measurements, typically results in hypersensitivity near the boundary, leading to the better quantitative accuracy in recovering the targets near the boundary.[29] Moreover, for the cases considered here (target being either in the interior of the domain or near the boundary), the linear iterative method is capable of recovering better contrast (modulo an error ~10%; see Fig. 3) when the reference contrast is 5:1. Nevertheless, the nonlinear iterative method may perform better in producing reconstructions with lesser variance and error in the reconstructed mean of the targets. Also, the plots in Fig. 5 of the data-model misfit and the rms error (versus iteration number) reveal that the nonlinear iterative methods perform substantially better than their linear counterparts in terms of image quality [at least by 30% in rms error, Fig. 5(b)] and in minimizing the data-model misfit [Fig. 5(a)]. Also, there is always a linear relationship between the contrast recovery and size of the target, which is well discussed in the literature.[23,30] The present study is conducted primarily to show that, in the case of dynamical contrast recovery, linear iterative methods provide a computationally efficient, yet reasonably accurate alternative to the recovery of the time varying updates. Note that Newton-based approaches, based on local linearization of the nonlinear functional, typically requires the initial guess to be within close neighborhood of the actual solution and may thus lead to limited contrast recovery. Deducing appropriate measures of such neighborhood is however beyond the scope of this work.

For data with 1% noise, the proposed SVD method results in nearly identical reconstructions to those via the linear iterative method, as seen from Figs. 4(b) and 4(c). The efficient Jacobian-reduced scheme, implemented within the linear iterative and SVD methods, has also given similar results (the error is less than 1%). A similar trend continues even when the data noise level is varied from 0% to 4% (the results are not shown here). We have also compared the behavior of the linear iterative, SVD, linear efficient, and SVD efficient methods over the iterations to convergence *vis-à-vis* the nonlinear method. The results are shown in Fig. 5 wherein the plotted L^2 error norms versus the iteration number via linear iterative methods are almost indistinguishable.

The computational efficacy of the proposed SVD method is evident from Fig. 6. The leading order of the number of operations in each method is given in Appendix B. The SVD of the Jacobian has made the reconstruction process to be of $O(NN^2)$ in contrast with $O(NN^3)$ flops needed for a traditional matrix inversion. It can be also seen that the computational complexity of the nonlinear method, which is $O(NN^6)$, makes it less attractive for rapid reconstructions necessary for dynamic NIR tomography applications. For a typical case with 1000 nodes, one can reconstruct 5 frames/s with the SVD method, 4 frames/s with the linear iterative method, and 1 frame/s with the nonlinear method. If a 200-node mesh is considered, the SVD method can reconstruct 15 frames/s making the image reconstruction procedure also nearly video-rate. It is shown that the reduction in computational complexity is larger for SVD as the number of nodes increases (compare $O(NN^2)$, $O(NN^3)$, and $O(NN^6)$ flops required for the SVD, linear iterative, and nonlinear methods, respectively). Even though the presented results are for the chosen set of optical properties and circular shape of the domain, the trends and computational efficacy of the algorithms are independent of the imaging domain size, shape, and optical properties.

The in-sync image reconstruction with data acquisition for rapid dynamic NIR tomography is determined by data transfer, any preprocessing to transform the raw data suitable for starting the image reconstruction, and the iterative procedure for recovering the tissue optical properties. In most approaches of NIR tomography, the pre-reconstruction factors have little impact on the overall image recovery speed; but as the speed of iterative reconstruction is improved, the impact of these pre-reconstruction factors would emerge, especially when specifically large sets of measurements are necessary. Recently, approaches of rapid NIR tomography have been extended to noninvasive imaging of internal tissues, such as prostate and rectum.[31] These internal imaging applications are in critical need of rapid image reconstruction. In these contexts, the SVD efficient method may provide a viable platform for such applications of rapid NIR tomography. Attempts are underway to use the SVD efficient method in the clinical/preclinical settings and estimate the efficacy of the algorithm compared to traditional algorithms.

V. CONCLUSIONS

In conclusion, the singular value decomposition of the Jacobian has led to a computationally efficient reconstruction algorithm, enabling the rapid dynamic NIR tomography image reconstruction procedure match the timeline of data acquisition (making it nearly video-rate). The SVD-based algorithm has made the number of operations in the image reconstruction procedure to be of $O(NN^2)$, rather than of $O(NN^3)$ (NN being the number of unknown parameters). The SVD-based algorithm has been tested and shown to be equivalent to the linear iterative algorithm both analytically and numerically using two-dimensional test examples. The SVD method has also been used for reconstruction based on a dynamic experimental data set to show its efficacy. If the initial guess is reasonably close to actual solution (which can be obtained through data calibration procedure), both linear and nonlinear iterative methods are capable of recovering almost the same contrast, with the linear iterative algorithms offering a computationally more efficient route [number of operations for linear iterative algorithms, $O(NN^3)$ and nonlinear algorithms, $O(NN^6)$].

ACKNOWLEDGMENTS

P.K.Y. acknowledges the IISc start-up grant [Grant No. IISc-Part(2A) Eleventh plan, 23/SERC] and the Apple Laureate award.

APPENDIX A: UPDATE EQUATION FOR μ_a USING SVD DECOMPOSITION

Putting $J^0 = USV^T$ (SVD decomposition of Jacobian) in Eq. (6), we will get

$$[(VSU^T * USV^T) + \alpha^i I]\Delta\mu^i = VSU^T * \delta^{i-1} \quad (S^T = S), \tag{A1}$$

$$[(VS^2V^T) + \alpha^i I]\Delta\mu^i = VSU^T * \delta^{i-1} \quad (U^TU = I). \tag{A2}$$

Multiplying both sides by V^T leads to

$$[V^T * (VS^2V^T) + V^T\alpha^i I]\Delta\mu = V^T * VSU^T * \delta^{i-1}, \tag{A3}$$

$$V^T * (S^2 + \alpha^i I) * \Delta\mu = SU^{T*}\delta^{i-1} \quad (V^TV = I), \tag{A4}$$

$$\Delta\mu^i = V * \Sigma^i * U^T * \delta^{i-1} \quad (V^T = V^{-1}), \tag{A5}$$

where

$$\sum_{lm}^{i} = \begin{cases} \dfrac{S_l}{S_l^2 + \alpha^i} & \text{if } l = m \\ 0 & \text{if } l \neq m \end{cases}.$$

APPENDIX B: CALCULATION OF NUMBER OF OPERATIONS FOR NONLINEAR ITERATIVE, LINEAR ITERATIVE, SVD METHODS

Typical calculation of number of operations will take into account only divisions and multiplications, ignoring additions. Note that the matrix inversion needed in the update equation was performed using Gaussian elimination. Typically, Gaussian elimination for an $N \times N$ matrix requires $((N^3/3) + N^2 - (N/3))$ operations.[26]

For the nonlinear iterative update equation [Eq. (5)], the number of operations required for iteration i is (ignoring the additions)

$$\text{Number of operations} = (NN^3/3) + NN^2 - (NN/3) + NN * NM^2. \tag{B1}$$

The leading order for the nonlinear iterative update equation is $O(NN^3)$. For nonlinear method, there is an additional computational cost of calculating Jacobian at every iteration, which is $O(NN^3)$, making the leading order as $O(NN^6)$.

For the linear iterative update equation [Eq. (6)], the number of operations required for iteration i is

$$\text{Number of operations} = (NN^3/3) + NN^2 - (NN/3). \tag{B2}$$

The leading order for the linear iterative update equation is $O(NN^3)$.

For the SVD update equation [Eq. (8)], the number of operations required for iteration i is

$$\text{Number of operations} = NN^2 + NN^2 + NN * NM^2. \tag{B3}$$

The leading order for SVD update equation is $O(NN^2)$.

[a]Electronic mail: phani@serc.iisc.ernet.in

[1]S. R. Arridge, "Optical tomography in medical imaging," Inverse Probl. **15**, R41–R93 (1999).
[2]N. Shah, A. Cerussi, C. Eker, J. Espinoza, J. Butler, J. Fishkin, R. Hornung, and B. Tromberg, "Noninvasive functional optical spectroscopy of human breast tissue," Proc. Natl. Acad. Sci. U.S.A. **98**, 4420–4425 (2001).
[3]S. Srinivasan, B. W. Pogue, S. Jiang, H. Dehghani, C. Kogel, S. Soho, J. J. Gibson, T. D. Tosteson, S. P. Poplack, and K. D. Paulsen, "Interpreting hemoglobin and water concentration, oxygen saturation and scattering measured in vivo by near-infrared breast tomography," Proc. Natl. Acad. Sci. U.S.A. **100**, 12349–12354 (2003).
[4]D. R. Leff, O. J. Warren, L. C. Enfield, A. Gibson, T. Athanasiou, D. K. Pattenl, J. C. Hebden, G. Z. Yang, and A. Darzi, "Diffuse optical imaging of the healthy and diseased breast: A systematic review," Breast Cancer Res. Treat. **108**, 9–22 (2008).
[5]J. S. Wyatt, "Cerebral oxygenation and haemodynamics in the foetus and newborn infant," Philos. Trans. R. Soc. London, Ser. B **352**, 697–700 (1997).
[6]D. A. Boas, D. H. Brooks, E. L. Miller, C. A. DiMarzio, M. Kilmer, R. J. Gaudette, and Q. Zhang, "Imaging the body with diffuse optical tomography," IEEE Signal Process. Mag. **18**, 57–75 (2001).
[7]B. W. Zeff, B. R. White, H. Dehghani, B. L. Schlaggar, and J. P. Culver, "Retinotopic mapping of adult human visual cortex with high-density diffuse optical tomography," Proc. Natl. Acad. Sci. U.S.A. **104**, 12169–12174 (2007).
[8]C. H. Schmitz, M. Löcker, J. M. Lasker, A. H. Hielscher, and R. L. Barbour, "Instrumentation for fast functional optical tomography," Rev. Sci. Instrum. **73**, 429 (2002).
[9]C. H. Schmitz, H. L. Graber, Y. Pei, M. Farber, M. Stewart, R. D. Levina, M. B. Levin, Y. Xu, and R. L. Barbour, "Dynamic studies of small animals with a four-color diffuse optical tomography imager," Rev. Sci. Instrum. **76**, 094302–094317 (2005).
[10]D. Piao, S. Jiang, S. Srinivasan, H. Dehghani, and B. W. Pogue, "Video-rate near-infrared optical tomography using spectrally encoded parallel light delivery," Opt. Lett. **30**, 2593–2595 (2005).
[11]D. Piao, H. Dehghani, S. Jiang, S. Srinivasan, and B. W. Pogue, "Instrumentation for video-rate near-infrared diffuse optical tomography," Rev. Sci. Instrum. **76**, 124301–124313 (2005).
[12]D. Piao and B. W. Pogue, "Rapid near-infrared diffuse tomography for hemodynamic imaging using a low-coherence wideband light source," J. Biomed. Opt. **12**, 014016 (2007).
[13]Y. Pei, H. L. Graber, and R. L. Barbour, "A fast reconstruction algorithm for implementation of time-series DC optical tomography," Proc. SPIE **4955**, 236–245 (2003).
[14]R. L. Barbour, H. L. Graber, Y. Xu, Y. Pei, and R. Aronson, "Strategies for imaging diffusing media," Transp. Theory Stat. Phys. **33**, 361–371 (2004).
[15]B. W. Pogue, X. Song, T. D. Tosteson, T. O. McBride, S. Jiang, and K. D. Paulsen, "Statistical analysis of non-linearly reconstructed near-infrared tomographic images: Part I-Theory and Simulation," IEEE Trans. Med. Imaging **21**, 755–763 (2002).
[16]M. E. Eames, B. W. Pogue, P. K. Yalavarthy, and H. Dehghani, "An efficient Jacobian reduction method for diffuse optical image reconstruction," Opt. Express **15**, 15908–15919 (2007).
[17]S. R. Arridge, M. Schweiger, M. Hiraoka, and D. T. Delpy, "A finite element approach for modeling photon transport in tissue," Med. Phys. **20**, 299–309 (1993).
[18]S. R. Arridge and M. Schweiger, "Photon-measurement density functions. Part2: Finite-element-method calculations," Appl. Opt. **34**, 8026–8037 (1995).
[19]H. Dehghani, M. E. Eames, P. K. Yalavarthy, S. C. Davis, S. Srinivasan, C. M. Carpenter, B. W. Pogue, and K. D. Paulsen, "Near infrared optical tomography using NIRFAST: Algorithm for numerical model and image reconstruction," Commun. Numer. Methods Eng. **25**, 711–732 (2009).
[20]M. Schweiger, S. R. Arridge, M. Hiroaka, and D. T. Delpy, "The finite element model for the propagation of light in scattering media: Boundary and source conditions," Med. Phys. **22**, 1779–1792 (1995).
[21]P. K. Yalavarthy, B. W. Pogue, H. Dehghani, and K. D. Paulsen, "Weight-matrix structured regularization provides optimal generalized least-squares estimate in diffuse optical tomography," Med. Phys. **34**, 2085–2098 (2007).
[22]X. Song, B. W. Pogue, T. D. Tosteson, T. O. McBride, S. Jiang, and K. D. Paulsen, "Statistical analysis of nonlinearly reconstructed near-infrared tomographic images: Part II-Experimental interpretation," IEEE Trans. Med. Imaging **21**, 764–772 (2002).
[23]B. W. Pogue, C. Willscher, T. O. McBride, U. L. Osterberg, and K. D. Paulsen, "Contrast-detail analysis for detection and characterization with

near-infrared diffuse tomography," Med. Phys. **27**, 2693–2700 (2000).
[24]B. W. Pogue, K. D. Paulsen, H. Kaufman, and C. Abele, "Calibration of near infrared frequency-domain tissue spectroscopy for absolute absorption coefficient quantitation in neonatal head-simulating phantoms," J. Biomed. Opt. **5**, 182–93 (2000).
[25]S. Jiang, B. W. Pogue, T. O. McBride, M. M. Doyley, S. P. Poplack, and K. D. Paulsen, "Near-infrared breast tomography calibration with optoelastic tissue simulating phantoms," J. Electron. Imaging **12**, 613 (2003).
[26]J. R. Westlake, *A Handbook of Numerical Matrix Inversion and Solution of Linear Equations* (Wiley, New York, 1968).
[27]T. O. McBride, B. W. Pogue, S. Jiang, U. L. Osterberg, and K. D. Paulsen, "Development and calibration of a parallel modulated near-infrared tomography system for hemoglobin imaging in vivo," Rev. Sci. Instrum. **72**, 1817–1824 (2001).
[28]D. Boas, "A fundamental limitation of linearized algorithms for diffuse optical tomography," Opt. Express **1**, 404–413 (1997).
[29]P. K. Yalavarthy, H. Dehghani, B. W. Pogue, and K. D. Paulsen, "Critical computational aspects of near infrared circular tomographic imaging: Analysis of measurement number, mesh resolution and reconstruction basis," Opt. Express **14**, 6113–6127 (2006).
[30]X. Song, B. W. Pogue, M. Doyley, H. Dehghani, S. Jiang, T. D. Tosteson, S. P. Poplack, and K. D. Paulsen, "Automated region detection based on the contrast-to-noise ratio in near-infrared tomography," Appl. Opt. **43**, 1053–1062 (2004).
[31]D. Piao, H. Xie, W. Zhang, J. S. Krasinski, G. Zhang, H. Dehghani, and B. W. Pogue, "Endoscopic, rapid near-infrared optical tomography," Opt. Lett. **31**, 2876–2878 (2006).